Journal of Molecular Structure 1180 (2019) 505–511

Contents lists available at ScienceDirect

Journal of Molecular Structure

journal homepage: http://www.elsevier.com/locate/molstruc

Monitoring the characteristic properties of Ga-doped ZnO by Raman spectroscopy and atomic scale calculations

Seyda Horzum [a, *], Fadil Iyikanat [a], Ramazan Tuğrul Senger [a], Cem Çelebi [a], Mohamed Sbeta [b], Abdullah Yildiz [b], Tülay Serin [c]

[a] Department of Physics, Izmir Institute of Technology, 35430, Izmir, Turkey
[b] Department of Energy Systems Engineering, Faculty of Engineering and Natural Sciences, Yıldırım Beyazıt University, Ankara, Turkey
[c] Department of Engineering Physics, Ankara University, 06100, Ankara, Turkey

ARTICLE INFO

Article history:
Received 3 August 2018
Received in revised form
7 November 2018
Accepted 21 November 2018
Available online 5 December 2018

Keywords:
Thin films
Ga-doped ZnO
Raman spectroscopy
XRD
ab initio

ABSTRACT

We experimentally and theoretically study how the structural and vibrational properties of zinc oxide (ZnO) are modified upon Gallium (Ga) doping. The characteristics of Ga-doped ZnO thin films which are synthesized by sol-gel spin coating method on glass substrates are monitored by using X-ray diffraction (XRD) and Raman scattering measurements. For atomic-level understanding of the experimental findings state-of-the-art density functional theory (DFT) based calculations are also performed. DFT calculations reveal that both the substitution and adsorption of Ga atoms in ZnO are energetically possible and substitutional doping in ZnO is the most favourable scenario. XRD measurements show that all the films are in wurtzite structure and the crystallite size of the films decreases with increasing Ga doping. In addition, Raman analysis show that strong vibrational modes at about 100 and 441 cm^{-1} are associated with E_2^{low} and E_2^{high} phonon branches of ZnO, respectively. While the frequency of the E_2^{low} mode downshifts with increasing Ga concentration, the E_2^{high} phonon mode is not affected by the Ga doping. Furthermore, E_{Ga} phonon branch, stemming from the substituted Ga atoms, emerges at low frequencies. It is also seen that the Raman intensity of the E_{Ga} peak linearly increases with increasing Ga concentration. Experimental results on the vibrational properties are in good agreement with the *ab initio* phonon calculations.

1. Introduction

Metal oxide thin films have been known for many years are attractive materials for future technology. Zinc oxide (ZnO) which is one of the important metal oxide materials has been extensively studied by many researchers for decades due to its remarkable optoelectronic properties [1–4]. It is used in a various applications, such as solar cells, light-emitting diodes (LEDs), ultraviolet (UV) lasers and sensors [5–12].

For tuning the physical properties of ZnO thin films, doping is one of the efficient methods. It has been reported that doping with various atoms such as In, Al, Cu, Ni, etc. can be used to enhance and control the structural, electrical, vibrational and optical characteristics of ZnO thin films [13–19]. Sharma et al. reported fabrication of highly conductive and stable p-type ZnO via phosphorus doping [20]. Furthermore, Gondoni et al. [21] demonstrated how the correlation between electrical and optical properties of Al doped ZnO thin films can be used to evaluate energy gap, conduction band effective mass and transport mechanisms. Yildiz et al. [22] showed that the electron-electron interactions in ZnO is enhanced by increasing Sn density and there is a corresponding shrinkage in the band gap, for Sn doped films. In addition, Horzum et al. demonstrated that the electronic defect states originating from Cu atoms for Cu doped ZnO thin films. These films are optically inactive and the optical band gap is formed by the band edges that belong to ZnO crystal [23]. Ga-doped ZnO thin films were also studied recently [24–26]. Yamada et al. deposited Ga-doped ZnO thin films using RF magnetron sputtering method and investigated the positional distribution of electrical resistivity and crystalline lattice constant of films [27]. Moreover, the study of optical band gap shift in Ga-doped ZnO thin films based on the combination of experimental and first-principles calculations was presented by Wang et al. [28] The optical properties of Ga-doped ZnO films grown using

* Corresponding author.
E-mail address: seydahorzum@iyte.edu.tr (S. Horzum).

https://doi.org/10.1016/j.molstruc.2018.11.064
0022-2860/

metal organic chemical vapor deposition were investigated by Ye et al. [29] They reported a study on the Burstein-Moss and band-gap renormalization effects on the near-band-edge transition in films. Although most of the studies have focused on characteristics of doped ZnO thin films, there are few studies about Ga-doped ZnO thin film which are supported by DFT calculations. In this study, we investigated the effect of Ga dopants on the characteristic properties of ZnO thin films. The structural and vibrational properties of Ga-doped ZnO thin films were analyzed by XRD and Raman spectrometry. We proposed a feasible scenario to understand how the Ga atoms are doped in ZnO. It is an analysis of vibrational properties with Raman spectrum in Ga-doped ZnO thin films. Experimental results on Raman spectrum are inadequate for understand what kind of doping, so that they should be used with theoretical predictions. Consequently, we combined all of these results in our study.

2. Methodology

2.1. Experimental analysis

Ga-doped ZnO thin films with 1, 3, and 5 at. % Ga contents were deposited on ultrasonically cleaned square glass substrates by sol-gel spin coating method. The details of the preparation of the films were reported elsewhere [30]. The crystal structure of the films was analyzed by means of Rigaku Miniflex 600 Table Top Powder X-ray diffractometer. CuK_α radiation source with a wavelength of 0.154 nm was employed and the scanning range 2θ of the diffractometer was adjusted to 5-80^0. Raman measurements were performed by Horiba XploRA Raman spectrometer equipped with a confocal microscope. To gather Raman-scattered light, a 100× objective magnification (NA = 0.90) of an Olympus Bx41 transmission and reflection illumination microscope (Olympus, France) was used. The laser excitation of 532 nm with grating 1800 grooves/mm was employed in a spectral range of 50–700 cm^{-1}.

2.2. Details of computational approach

First principle calculations were carried out within the density functional theory (DFT) using the projector augmented wave (PAW) [31,32] potentials as implemented in the Vienna *ab initio* simulation package (VASP) [33,34]. The generalized gradient approximation (GGA) using the Perdew-Burke-Ernzerhof (PBE) functional was utilized for exchange-correlation energy [35]. In order to consider strong correlations between *d*-orbitals of Zn atoms and *p*-orbitals of O atoms, the DFT + U method defined by Dudarev was performed [36]. Within the GGA + U approach the on-site Coulomb parameter, *U*, and the exchange parameter, *J*, are combined into one effective interaction parameter $U_{\text{eff}} = U - J$. The plane-wave cutoff energy was set to be 500 eV. The convergence criterion for energy was chosen to be 10^{-5} eV. The total force in the unit cell was kept below 10^{-4} eV/Å. Pressure on the unit cell was decreased to values less than 1 kB. For the Brillouin Zone (BZ) integration, a $24 \times 24 \times 18$ Γ-centered mesh was used for the primitive cell. Analysis of the charge transfers on the atoms was made using Bader technique [37].

Phonon calculations were performed using the small displacement method as implemented in the PHON code [38]. The nonresonant Raman calculations were performed for undoped and various concentrations of Ga-doped ZnO crystals. A displacement of 0.015 Å was applied for phonon calculations and resulting dynamical matrix was obtained. The convergence of intensity of the Raman spectrum and frequencies of acoustical modes with respect to the k-point sampling and energy cutoff was carefully examined. The k-point sampling of $12 \times 12 \times 9$ was used for the Raman intensity calculation of the primitive cell. Therefore, for the calculation of the Raman activities of each mode were determent through the change in macroscopic dielectric tensor.

3. Results and discussion

3.1. Structural properties

In this section, we investigate how the structural properties of ZnO are modified upon Ga doping. First we determine whether the undoped ZnO structure is formed in wurtzite or zincblende phase. As shown in Fig. 1 (a), undoped ZnO has (100), (002), (101), (102), (110), (103), (200), (112), (201) and (004) peaks which correspond to hexagonal wurtzite ZnO and these peaks match the JCPDS card (zinc oxide, 80-0074). It is also seen from the XRD spectrum that the preferential orientation is along the (002) plane of the wurtzite ZnO. In order to obtain the lattice parameters more accurately the Rietveld refinement method is used and the parameters from the XRD spectrum are analyzed using the FullProf package. The values of lattice parameters (*a*, *c* and *c*/*a*), refined parameters (R_{wp}, R_p and χ^2) and the cell volume (*V*) obtained from XRD measurements by Rietveld refinement analyses are given in Table 1. The size of the crystallites with the (002) plane can be calculated using the Scherrer's formula. Neglecting the peak broadening due to residual stress in the films, the crystallite size is given by $D = 0.9\lambda/(\beta\cos\theta)$, where β is the amount of broadening in the diffraction peak at half its maximum intensity in radians (where λ is 1.54 Å). In addition, the Zn–O bond length is given by the following equation;

$$r_{Zn-O} = \left[\left(\frac{a^2}{3}\right) + (0.5 - u)^2 c^2\right]^{1/2} \quad (1)$$

where, $u=(a^2/3c^2)+0.25$ [39]. The calculated values of the

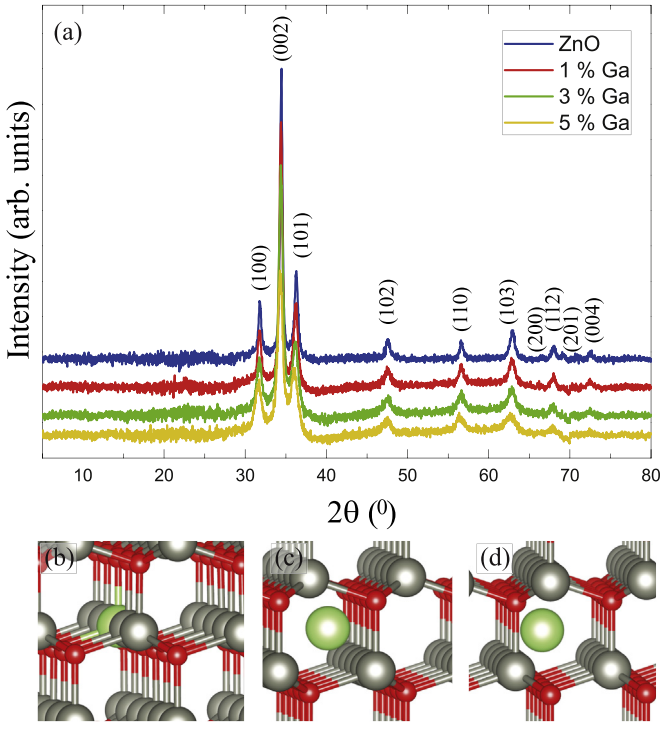

Fig. 1. (a) XRD spectrum of undoped and Ga-doped ZnO thin films. (b) Substitutional Ga instead of Zn, Ga atom in the (c) octahedral and (d) tetrahedral interstitial area of ZnO. The green, grey and red atoms are Ga, Zn and O atoms, respectively.

Table 1
The lattice parameters (a, c and c/a), refined parameters (R_{wp}, R_p and χ^2), crystallite size (D), cell volume (V), Zn–O bond length (r_{Zn-O}) calculated from XRD measurements by Rietveld refinement analyses, for undoped and Ga-doped ZnO films.

Doping (%)	a (Å)	c (Å)	c/a	R_{wp}	R_p	χ^2	D (Å)	V (Å^3)	r_{Zn-O} (Å)
undoped	3.2492(2)	5.2082(2)	1.603	7.28	5.92	1.61	222.90	47.614	1.977
1	3.2499(2)	5.2086(3)	1.603	6.39	5.03	1.38	167.86	47.641	1.978
3	3.2521(2)	5.2113(2)	1.600	5.45	4.32	1.22	164.07	47.731	1.979
5	3.2585(3)	5.2175(3)	1.600	5.98	4.50	1.36	113.96	47.976	1.983

crystallite size and the Zn–O bond length are given in Table 1.

We also theoretically study the structural properties of the undoped wurtzite ZnO crystal via *ab initio* DFT calculations. In the present work, the values of U_{eff} terms are employed as 1 eV and 12 eV for the d-orbitals of Zn atoms and the p-orbitals of O atoms, respectively. Therefore, as given in Table 2, the optimized lattice parameters of undoped ZnO are calculated to be $a = b = 3.244$ Å and $c = 5.230$ Å with c/a ratio of 1.61. The bond length between Zn and O atoms along c-axis and those of the planar bonds are 1.98 and 1.97 Å, respectively. Bader charge analysis shows that the bond between Zn and O is ionic-type with a charge depletion of 1.2e from Zn to O atom due to a difference in the electronegativities of Zn and O atoms (1.65 and 3.44 for Zn and O atoms, respectively).

In order to see the doping effects on the structural properties of ZnO, we investigate the XRD spectra of Ga-doped films (Fig. 1 (a)). According to the XRD patterns, similar peaks are observed as in undoped ZnO. Since Ga atoms are homogeneously incorporated into the ZnO matrix, there is no additional peaks in the XRD pattern. It is also observed that the intensity of diffraction peaks decreases by doping. In addition, the preferential orientation which is along the (002) plane stays unaltered with Ga doping.

While the structural phase and crystallite size can be obtained from the XRD spectrum, the question of how the wurtzite ZnO is doped by Ga atoms requires a theoretical investigation. In the DFT total energy calculations performed to determine the most favourable site for Ga atoms in the wurtzite ZnO, three different configurations are considered: two different types of interstitial doping (octahedral and tetrahedral) and one substitutional doping of a Zn atom by a Ga atom. The geometric structures of interstitial and substitutional Ga-doped wurtzite ZnO are shown in Fig. 1 (b), (c) and (d). A $3 \times 3 \times 2$ supercell of ZnO corresponding to a doping concentration of ~ 1.4% is used. It is found that the substitution of Zn with Ga is 48 and 57 meV per atom more favourable than the octahedral and tetrahedral interstitial sites, respectively. Thus, based on the total energy calculations, substitutional doping of Zn by Ga atoms is highly probable. In addition, previous studies revealed that substitutional doping of Ga atom in the wurtzite ZnO is more likely to occur [40,41]. Therefore, in the following we only consider the substitutional doping.

The substitution of Zn^{+2} by Ga^{+3}creates defects and distorts the local ordering of the crystal structure. It appears that the crystallite size of Ga-doped films is smaller than the undoped film. As the amount of doping increases, the crystallite size decreases due to the increase of lattice defects (Table 1). As shown in Table 1, the cell parameters and bond length (r_{Zn-O}) are expanded when compared to undoped ZnO. As consistented with experimental results, it is seen in DFT calculations that Ga doping enlarges the lattice parameters of ZnO. As given in Table 2, the lattice parameter of the structure is 3.247 and 3.252 for ~ 1.4% and ~ 3% doping concentrations, respectively. Bader charge analysis reveals that similar to the bond between Zn and O, the bond between Ga and O is also ionic with a charge donation of 1.0 e from Ga to O. It is found that the nonmagnetic structure of ZnO is unaffected by substitutional doping of Ga atoms.

Table 2
Calculated lattice parameters a and c, Bader charge donated by the adsorbed atoms (also Zn atom in the undoped structure).

Doping (%)	a (Å)	c (Å)	$\Delta\rho$ (e)
undoped	3.244	5.230	1.2
~ 1.4	3.247	5.245	1.0
~ 3.0	3.252	5.259	1.0

3.2. Vibrational properties

Raman spectra of undoped and Ga-doped ZnO shown in Fig. 2 possess two dominant peaks at 100 and 441 cm^{-1}. In addition, phonon dispersion and Raman activity analysis of wurtzite ZnO (calculated using $3 \times 3 \times 2$ supercell) are also shown in Fig. 3. The phonon spectra of the crystal have no imaginary frequencies which indicates the dynamical stability of the structure. As seen in Fig. 3 (b) there are 4 Raman active modes, one of which has a relatively low intensity. The phonon modes which we calculate at 97.2 and 415.4 cm^{-1} correspond to the modes at 100 and 441 cm^{-1} observed in the Raman spectrum and these modes are associated with E_2^{low} and E_2^{high} phonon modes of ZnO, respectively.

In the E_2 phonon modes, neighboring ions move opposite to each in the plane perpendicular to the c-axis. Therefore the total displacement and net polarization are zero and E_2^{low} and E_2^{high} modes are non-polar modes. E_2^{low} mode mostly involves the vibrations of Zn sub-lattice, while E_2^{high} mode predominantly occurs with motion of oxygen atoms [42]. Optical character and frequency of these modes are illustrated in Fig. 3 (b). A strong E_2^{high} mode is an indication of good crystallinity of wurtzite ZnO. According to Fig. 2, as Ga doping ratio increases, this mode becomes broader and less

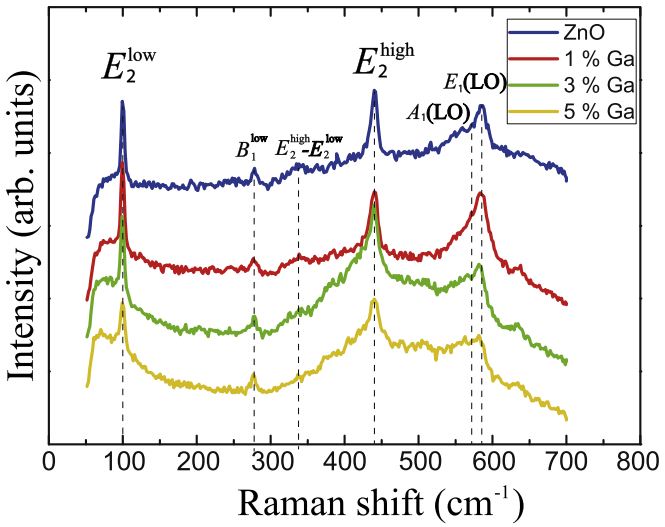

Fig. 2. Raman spectrum of undoped and Ga-doped ZnO thin films.

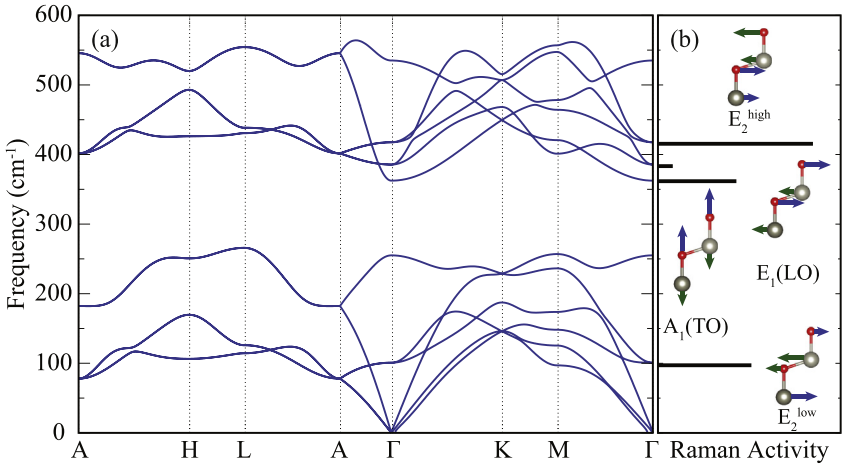

Fig. 3. (a) Phonon band diagram and corresponding (b) Raman activities of wurtzite ZnO crystal. Vibrational motion of individual atoms in some prominent Raman active modes are also shown. The green, grey and red atoms are Ga, Zn and O and atoms, respectively.

intense peaks and this indicates decline in the crystallinity of ZnO with Ga concentration. It is also seen that frequency of E_2^{high} mode almost remains unaltered with the Ga doping. The frequency of E_2^{high} mode which is located at 441 cm^{-1} in undoped ZnO shows a little shift to 440 cm^{-1} in 5% Ga-doped film. Similarly, DFT calculations exhibit that E_2^{high} mode slightly shifts to 415.3 and 413.8 cm^{-1} for 1.4% and 3% Ga doping, respectively. Since the E_2^{high} mode is dominantly related to the vibration of O atoms, the presence of Ga dopant atom negligibly changes the frequency of this mode.

In Fig. 2, it is seen that two peaks at around 573 and 584 cm^{-1} are combined in a single LO mode. These peaks are ascribed to A_1(LO) and E_1(LO) modes of ZnO, respectively. In A_1 and E_1 modes, which are oxygen dominated, the atoms move parallel and perpendicular to the *c*-axis, respectively. The neighboring ions move in the same direction in these phonon modes and displacement of the atoms causes a net polarization. Consequently, A_1 and E_1 modes are split into transverse optical (TO) and longitudinal optical (LO) phonons due to ionic character of Zn–O bonds. Except for a vague A_1(TO) mode obtained at 380 cm^{-1}, TO modes are absent in our measurements since the backscattered light is collected along the *c*-axis [43,44]. The reason why we see A_1(TO) mode in the Raman spectrum may be related to the polycrystalline character of the film. For highly oriented ZnO films, when the incident light is normal to the surface, E_2 and A_1(LO) modes can be monitored and other modes are forbidden due to the Raman selection rules [44]. The existence of E_1(LO) mode in all of the films can be attributed to the deterioration of the selection rule because of the use of the Raman microscope [7,45]. As seen in Fig. 2, the E_1(LO) mode at 584 cm^{-1} in the undoped and 1% Ga-doped ZnO shifts towards 582 cm^{-1} in 3% and 5% Ga-doped samples. We also observed that the peak width of E_1(LO) mode shrinks for the Ga-doped ZnO. E_1(LO) mode is ascribed to the oxygen vacancies in ZnO [46]. In addition, it is also seen that A_1(LO) mode separates from E_1(LO) as the Ga doping ratio increases. The peak observed around 572 cm^{-1} for 1% Ga, shifts to 563 cm^{-1} in 5% Ga-doped ZnO. A_1(LO) mode may stem from intrinsic defects of oxygen vacancies and interstitial zinc cations [47]. The calculated phonon mode spectra agree well with the experimental results. (E_2^{low}, A_1(TO), and E_2^{high} modes are experimentally detected at 100, 380, 441 cm^{-1}). However, we calculate the energy of the E_1(LO) mode quite shifted compared to the experimental results. This inaccuracy stems from the large LO-TO splitting of wurtzite ZnO crystal [48]. Standart DFT methods may provide severely incorrect results in calculating high-energy modes of a polar material like ZnO. However, in the present study we focus on the low-frequency phonon modes, where the methodology is quite reliable.

In addition to prominent modes, the anomalous Raman modes at 275, 335 and 631 cm^{-1} are also monitored in Raman spectrum of undoped ZnO. The peak at 275 cm^{-1} is the silent mode $B_1{}^{low}$ while the other modes are second-order modes or multi-phonon processes. As seen in Fig. 2, the $B_1{}^{low}$ mode remains unchanged with Ga doping. Furthermore, it is observed that the broad peak at 335 cm^{-1} which corresponds to E_2^{high}-E_2^{low} disappears as the Ga concentration increases. Additionally, as displayed in Fig. 2, the mode which is observed at 631 cm^{-1} in undoped ZnO shifts to 624 cm^{-1} in 5% Ga-doped film. The same mode was observed for Ga and Sb doped ZnO in previous reports [49,50]. It can be related to the defects rather than the Ga doping. The observation of some anomalous modes in the Raman spectra of ZnO films can be ascribed to the disorder-activated Raman scattering [51,52]. This scattering can be stimulated by the distortion of the lattice symmetry due to defects or impurities [51].

In this section, Ga doping dependency of the dynamical stability of the ZnO is also investigated. Calculated phonon eigenfrequencies that have real eigenvalues in the whole Brillouin zone indicate the dynamical stability of Ga-doped ZnO. The phonon dispersions of 1.4%, 3%, 6% and 12% Ga-doped ZnO are shown in Fig. 4. It appears that the structure is dynamically stable for 1.4%, 3% and 6% doped cases, however over-doped case of 12% leads to dynamical instability. It is clearly seen that all the mode frequencies display softening with increasing amount of doping. Since Ga doping increases the lattice parameter, the bonds of the material weaken and this leads to a decrease in the mode frequencies. It is found that the large phonon band gap of ZnO between the frequencies of ~ 250 and ~ 350 cm^{-1} is not affected by Ga doping.

Moreover, as seen in Fig. 2 when the Ga doping increases, an additional peak arises with a lower frequency than that of E_2^{low}. It is clearly seen that the Raman intensities of the extra peak (E_{Ga}) and E_2^{low} are strongly dependent on the amount of Ga doping. To further understand the doping effect in the low-frequency regime, doping dependencies of these two modes are examined in detail both experimentally and theoretically. DFT calculations also revealed that when the ZnO crystal is doped with Ga, an additional Raman

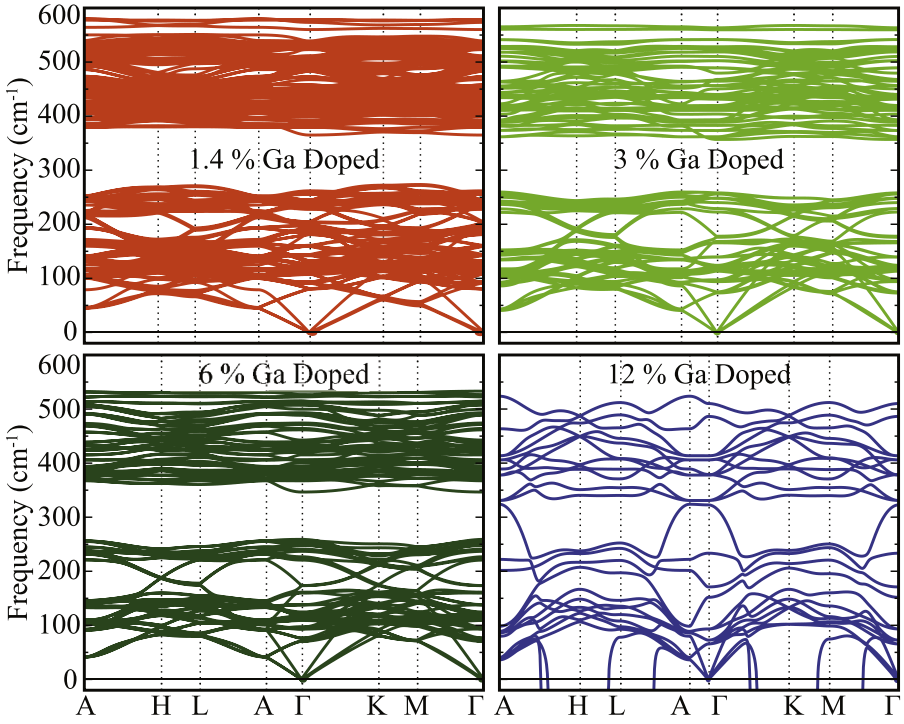

Fig. 4. Phonon band dispersions with respect to the doping amount.

active mode appears in the low-frequency regime. Calculated doping-dependent Raman intensity and optical character of E_{Ga} and E_2^{low} are illustrated in Fig. 5. As seen in the figure, E_{Ga} is characterized by a counter-phase motion of layers of four atomic thickness. For the sake of comparision Gaussian fitting of the measured Raman intensities of these two modes are performed and shown in the inset of the Fig. 5. The frequencies of E_{Ga} and E_2^{low} are measured as 74 and ~ 99.6 cm^{-1} for 1% Ga doping, respectively. It is clearly seen that the downshift in the frequency of E_{Ga} and E_2^{low} occurs when the amount of Ga doping increases (Table 3). DFT calculations

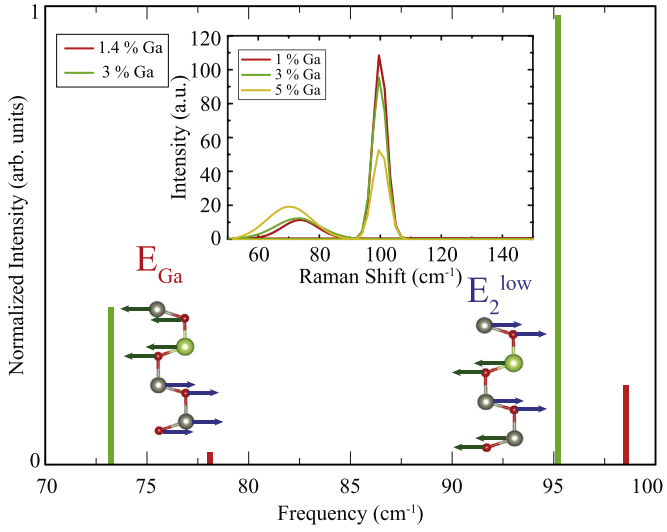

Fig. 5. Doping dependency of the Raman activity of E_{Ga} and E_2^{low} modes. Side views of atomic displacements of E_{Ga} and E_2^{low} modes are shown. The green, grey and red atoms are Ga, Zn and O atoms, respectively. Inset: Presentation of Baseline and Gauss fitting for E_{Ga} and E_2^{low} peaks.

also show a similar phonon softening trend. It is found that as the Ga doping increases from ~ 1.4% to ~ 3.0%, the frequency of the E_{Ga} and E_2^{low} decreases from 78.1 to 97.0 cm^{-1} to 73.2 and 95.2 cm^{-1}, respectively. The existence of Ga atoms in the ZnO lattice causes a change in the vibrational frequency of the E_2^{low} mode. Since the E_2^{low} mode is associated with vibration of Zn atoms, substitutional doping of the Zn atoms changes the vibrational frequencies of the Ga-doped films. In order to understand the doping-level dependence of the additional peak, we calculated the intensity ratio of the two peaks, E_{Ga} and E_2^{low}. As seen in the inset of Fig. 5 and Table 3, there is a significant relationship between the amount of Ga doping and the changes in the intensity ratio of these two peaks. The intensity ratio, $I_{E_{Ga}}/I_{E_2^{low}}$, is measured as 0.11, 0.43, and 0.65 for 1%, 3% and 5% Ga-doped samples, respectively. We found a similar trend in the theoretical calculations. As the amount of Ga doping increases from 1.4% to 3%, the ratio, $I_{E_{Ga}}/I_{E_2^{low}}$, increases from 0.11 to 0.35. The change in the relative intensity ratio depending on the amount of doping can be attributed to the increase in the lattice constant. As the doping amount increases, the lattice constant of the crystal increases and consequently, the dipole between oppositely vibrating atoms of interlayer modes enhances. Since the dipole between oppositely vibrating atoms of E_{Ga} mode is larger than that of the E_2^{low} mode, polarizability of the E_{Ga} mode is higher. As a result, the Ga doping enhances the intensity of the E_{Ga} more than the E_2^{low} mode. Therefore, the doping dependence of Raman intensities and peak positions of E_{Ga} and E_2^{low} modes can be used as a measure of the amount of doping in the material.

4. Conclusions

In this study, in order to examine the doping effects on the characteristic properties of ZnO thin films, undoped and Ga-doped films were grown on glass substrates by sol-gel spin coating

Table 3
$I_{E_{Ga}}/I_{E_2^{low}}$ peak ratios of experimental and DFT results.

Doping (%)	Experimental Results			Doping (%)	DFT Results		
	E_{Ga} (cm^{-1})	E_2^{low} (cm^{-1})	$I_{E_{Ga}}/I_{E_2^{low}}$		E_{Ga} (cm^{-1})	E_2^{low} (cm^{-1})	$I_{E_{Ga}}/I_{E_2^{low}}$
1	74	99.6	0.11	1.4	78.1	97.0	0.11
3	72	99.1	0.43	3.0	73.2	95.2	0.35
5	70	98.5	0.65				

method. The structural and vibrational properties of the films were investigated by performing both measurements and *ab initio* DFT calculations. The XRD spectra indicated that the films have hexagonal wurtzite structure and all of the films exhibit *c*-axis oriented in the (002) plane. Ga doping induces a slight increase in the lattice parameters and a decrease in the crystallite size of the films. DFT calculations revealed that the most favourable configuration for a Ga dopant atom is to substitute a Zn site. Bader charge analysis showed that bond between Ga and O is ionic with a charge donation of 1.0 e from Ga to O. Raman measurements demonstrated that two dominant vibrational modes at around 100 and 441 cm^{-1} are associated with E_2^{low} and E_2^{high} phonon modes of ZnO, respectively. Strong E_2^{high} mode indicated wurtzite ZnO lattice. As the Ga concentration increases, it is observed that the frequency of E_2^{low} mode downshifts while the frequency of E_2^{high} almost remains unaltered. Since E_2^{low} mode is related to the vibration of Zn atoms, substitution of Ga dopant atom with Zn atom might shift the vibrational frequencies of the E_2^{low}. DFT calculations also revealed 4 Raman active modes of ZnO at 97, 362, 383 and 415 cm^{-1}. These phonon modes are associated with E_2^{low}, A_1(TO), E_1(LO) and E_2^{high} vibrational modes. The calculated phonon mode frequencies agree well with the experimental results, except for E_1(LO) at 383 cm^{-1} due to large LO-TO splitting of wurtzite ZnO crystal. Moreover, we observed that an additional peak appeared with Ga doping at low frequency values. It was seen that while this additional peak is at around 74 cm^{-1} in 1% Ga-doped, it shifts to 70 cm^{-1} in 5% Ga-doped films. Phonon calculations confirmed this additional phonon mode which is obtained at low frequency. In addition, the intensity ratio of phonon modes of E_{Ga} and E_2^{low} which are obtained at low frequency increases from 0.11 to 0.65 in 1% and 5% Ga-doped, respectively. DFT calculations also demonstrated a similar trend in Ga-doped ZnO. Our results manifested that Raman analysis and theoretical phonon calculations are efficient methods for understanding the effect of doping in ZnO.

Acknowledgments

This work was supported by TUBITAK-BIDEB 2218-National Postdoctoral Research Scholarship Programme. Computational resources were provided by TUBITAK ULAKBIM, High Performance and Grid Computing Center (TR-Grid e-Infrastructure).

References

[1] S.P.S. Porto, B. Tell, T.C. Damen, Near-forward Raman scattering in zinc oxide, Phys. Rev. Lett. 16 (1966) 450–453.
[2] D.C. Look, D.C. Reynolds, J.W. Hemsky, R.L. Jones, J.R. Sizelove, Production and annealing of electron irradiation damage in ZnO, Appl. Phys. Lett. 75 (1999) 811–813.
[3] Ü. Özgür, Y.I. Alivov, C. Liu, A. Teke, M.A. Reshchikov, S. Doğan, V. Avrutin, S.-J. Cho, H. Morkoç, A comprehensive review of ZnO materials and devices, J. Appl. Phys. 98 (2005) 11.
[4] S.J. Pearton, D.P. Norton, K. Ip, Y.W. Heo, T. Steiner, Recent advances in processing of ZnO, J. Vac. Sci. Technol. B 22 (2004) 932–948.
[5] P.F. Carcia, R.S. McLean, M.H. Reilly, G. Nunes, Transparent ZnO thin-film transistor fabricated by rf magnetron sputtering, Appl. Phys. Lett. 82 (2003) 1117–1119.
[6] R.L. Hoffman, B.J. Norris, J.F. Wager, ZnO-based transparent thin-film transistors, Appl. Phys. Lett. 82 (2003) 733–735.
[7] H. Morkoç, Ü. Özgür, Zinc Oxide: Fundamentals, Materials and Device Technology, Willey-VCH publish, 2008.
[8] Ü. Özgür, D. Hofstetter, H. Morkoç, ZnO devices and applications: a review of current status and future prospect, Proc. IEEE 98 (2010) 1255–1268.
[9] Q.A. Xu, J.W. Zhang, K.R. Ju, X.D. Yang, X. Hou, ZnO thin film photoconductive ultraviolet detector with fast photoresponse, J. Cryst. Growth 289 (2006) 44–47.
[10] I.E. Titkov, L.A. Delimova, A.S. Zubrilov, N.V. Seredova, I.A. Liniichuk, I.V. Grekhov, ZnO/GaN heterostructure for LED applications, J. Mod. Optic. 56 (2009) 653–660.
[11] S.-H. Nam, M.-H. Kim, D.G. Yoo, S.H. Jeong, D.Y. Kim, N.-E. Lee, J.-H. Boo, Metal-doped ZnO thin films: synthesis, etching characteristic, and application test for organic light emitting diode (oled) devices, Surf. Rev. Lett. 17 (2010) 121–127.
[12] S. Sharma, C. Periasamy, A study on the electrical characteristic of n-ZnO/p-Si heterojunction diode prepared by vacuum coating technique, Superlattice. Microst. 73 (2014) 12–21.
[13] S. Palimar, K.V. Bangera, G.K. Shivakumar, Study of the doping of thermally evaporated zinc oxide thin films with indium and indium oxide, Appl. Nanosci. 3 (2013) 549–553.
[14] Y.-S. Kim, W.-P. Tai, Electrical and optical properties of Al-doped ZnO thin films by solgel process, Appl. Surf. Sci. 253 (2007) 4911–4916.
[15] T. Prabhakar, L. Dai, L. Zhang, R. Yang, L. Li, T. Guo, Y. Yan, Effects of growth process on the optical and electrical properties in Al-doped ZnO thin films, J. Appl. Phys. 115 (2014), 083702.
[16] C.-H. Hsu, L.-C. Chen, X. Zhang, Effect of the Cu source on optical properties of CuZnO films deposited by ultrasonic spraying, Materials 7 (2014) 1261–1270.
[17] R. Siddheswaran, M. Netrvalová, J. Savková, P. Novák, J. Ocenášek, P. Šutta, J. Kovác Jr., R. Jayavel, Reactive magnetron sputtering of Ni doped ZnO thin film: investigation of optical, structural, mechanical and magnetic properties, J. Alloy. Comp. 636 (2015) 85–92.
[18] P. Prunici, F.U. Hamelmann, W. Beyer, H. Kurz, H. Stiebig, Modelling of infrared optical constants for polycrystalline low pressure chemical vapour deposition ZnO:B films, J. Appl. Phys. 113 (2013) 123104.
[19] Amit K. Das, R.S. Ajimsha, L.M. Kukreja, Quantum corrections to temperature dependent electrical conductivity of ZnO thin films degenerately doped with Si, Appl. Phys. Lett. 104 (2014), 042112.
[20] P. Sharma, Aaryashree, V. Garg, S. Mukherjee, Optoelectronic properties of phosphorus doped p-type ZnO films grown by dual ion beam sputtering, J. Appl. Phys. 121 (2017) 225306.
[21] P. Gondoni, M. Ghidelli, F. Di Fonzo, M. Carminati, V. Russo, A. Li Bassi, C.S. Casari, Structure-dependent optical and electrical transport properties of nanostructured Al-doped ZnO, Nanotechnology 23 (2012) 365706.
[22] A. Yildiz, E. Ozturk, A. Atilgan, M. Sbeta, A. Atli, T. Serin, An understanding of the band gap shrinkage in Sn-doped ZnO for dye-sensitized solar cells, J. Electron. Mater. 46 (2017) 6739–6744.
[23] S. Horzum, E. Torun, T. Serin, F.M. Peeters, Structural, electronic and optical properties of Cu-doped ZnO: experimental and theoretical investigation, Philos. Mag. 96 (2016) 1743–1756.
[24] E. Šermukšnis, J. Liberis, M. Ramonas, A. Matulionis, M. Toporkov, H.Y. Liu, V. Avrutin, Ü. Özgür, H. Morkoç, Hot-electron energy relaxation time in Ga-doped ZnO films, J. Appl. Phys. 117 (2015), 065704.
[25] S. Chen, M.E.A. Warwick, R. Binions, Effects of film thickness and thermal treatment on the structural and opto-electronic properties of Ga-doped ZnO films deposited by solgel method, Sol. Energy Mater. Sol. Cells 137 (2015) 202–209.
[26] M. Gabás, P. Torelli, N.T. Barrett, M. Sacchi, J.R.R. Barrado, Electronic structure of Al-and Ga-doped ZnO films studied by hard X-ray photoelectron spectroscopy, Apl. Mater. 2 (2014), 012112.
[27] Y. Yamada, K. Kadowaki, H. Kikuchi, S. Funaki, S. Kubo, Positional variation and annealing effect in magnetron sputtered Ga-doped ZnO films, Thin Solid Films 609 (2016) 25–29.
[28] Y. Wang, W. Tang, J. Liu, L. Zhang, Stress-induced anomalous shift of optical band gap in Ga-doped ZnO thin films: experimental and first-principles study, Appl. Phys. Lett. 106 (2015) 162101.
[29] J.D. Ye, S.L. Gu, S.M. Zhu, S.M. Liu, Y.D. Zheng, R. Zhang, Y. Shi, Fermi-level band filling and band-gap renormalization in Ga-doped ZnO, Appl. Phys. Lett. 86 (2005) 192111.
[30] M. Sbeta, T. Serin, A. Yildiz, Determination ofthecritical Carrier concentration

forthemetal-insulator transition inGa-doped ZnO, J. Mater. Sci. Mater. Electron. (2018). https://doi.org/10.1007/s10854-018-9543-9.
[31] G. Kresse, D. Joubert, From ultrasoft pseudopotentials to the projector augmented-wave method, Phys. Rev. B 59 (1999) 1758–1775.
[32] P.E. Blöchl, Projector augmented-wave method, Phys. Rev. B 50 (1994) 17953–17979.
[33] G. Kresse, J. Hafner, Ab initio molecular dynamics for liquid metals, Phys. Rev. B 47 (1993) 558–561.
[34] G. Kresse, J. Furthmüller, Efficient iterative schemes for ab initio total-energy calculations using a plane-wave basis set, Phys. Rev. B 54 (1996) 11169–11186.
[35] J.P. Perdew, K. Burke, M. Ernzerhof, Generalized gradient approximation made simple, Phys. Rev. Lett. 77 (1996) 3865–3868.
[36] S.L. Dudarev, G.A. Botton, S.Y. Savrasov, C.J. Humphreys, A.P. Sutton, Electron-energy-loss spectra and the structural stability of nickel oxide: an LSDA+U study, Phys. Rev. B 57 (1998) 1505–1509.
[37] G. Henkelman, A. Arnaldsson, H. Jónsson, A fast and robust algorithm for Bader decomposition of charge density, Comput. Mater. Sci. 36 (2006) 354–360.
[38] D. Alfè, PHON: a program to calculate phonons using the small displacement method, Comput. Phys. Commun. 180 (2009) 2622–2633.
[39] B.D. Cullity, Elements of X-ray Diffraction, Addison-Wesley Publishing Company, Inc., Boston, 1956.
[40] H.I. Berrezoug, A.E. Merad, M. Aillerie, A. Zerga, First principle study of structural stability, electronic structure and optical properties of Ga doped ZnO with different concentrations, Mater. Res. Express 4 (2017), 035901.
[41] E.M. Proupin, P. Palacios, P. Wahnón, Electronic and atomic structure of complex defects in Al- and Ga-highly doped ZnO films, Mater. Chem. Phys. 160 (2015) 420–428.
[42] J.M. Calleja, Manuel Cardona, Resonant Raman scattering in ZnO, Phys. Rev. B 16 (1977) 3753–3761.
[43] M. Gabás, A. Landa-Cánovas, J. Luis Costa-Krämer, F. Agulló-Rueda, Agustín R. González-Elipe, P. Díaz-Carrasco, J. Hernández-Moro, I. Lorite, P. Herrero, P. Castillero, A. Barranco, J. Ramón Ramos-Barrado, Differences in n-type doping efficiency between Al- and Ga-ZnO films, J. Appl. Phys. 113 (2013) 163709.
[44] Y. Zhang, H. Jia, R. Wang, C. Chen, X. Luo, D. Yu, C. Lee, Low-temperature growth and Raman scattering study of vertically aligned ZnO nanowires on Si substrate, Appl. Phys. Lett. 83 (2003) 4631–4633.
[45] N. Ashkenov, B.N. Mbenkum, C. Bundesmann, V. Riede, M. Lorenz, D. Spemann, E.M. Kaidashev, A. Kasic, M. Schubert, M. Grundmann, G. Wagner, H. Neumann, V. Darakchieva, H. Arwin, B. Monemar, Infrared dielectric functions and phonon modes of high-quality ZnO films, J. Appl. Phys. 93 (2003) 126–133.
[46] F. Rubio-Marcos, C.V. Manzano, J.J. Reinosa, I. Lorite, J.J. Romero, J.F. Fernández, M.S. Martín-González, Modification of optical properties in ZnO particles by surface deposition and anchoring of NiO nanoparticles, J. Alloy. Comp. 509 (2011) 2891–2896.
[47] S.K. Sharma, G.J. Exarhos, Raman spectroscopic investigation of ZnO and doped ZnO films, nanoparticles and bulk material at ambient and high pressures, Solid State Phenom. 55 (1997) 32–37.
[48] A. Calzolari, M.B. Nardelli, Dielectric properties and Raman spectra of ZnO from a first principles finite-differences/finite-fields approach, Sci. Rep. 3 (2013) 2999.
[49] C. Bundesmann, N. Ashkenov, M. Schubert, D. Spemann, T. Butz, E.M. Kaidashev, M. Lorenz, M. Grundmann, Raman scattering in ZnO thin films doped with Fe, Sb, Al, Ga, and Li, Appl. Phys. Lett. 83 (2003) 1974–1976.
[50] A. Escobedo-Morales, U. Pal, Effect of In, Sb and Ga doping on the structure and vibrational modes of hydrothermally grown ZnO nanostructures, Curr. Appl. Phys. 11 (2011) 525–531.
[51] F.J. Manjón, B. Marí, J. Serrano, A.H. Romero, Silent Raman modes in zinc oxide and related nitrides, J. Appl. Phys. 97 (2005), 053516.
[52] C. Lung, M. Toma, M. Pop, D. Marconi, A. Pop, Characterization of the structural and optical properties of ZnO thin films doped with Ga, Al and (Al+Ga), J. Alloy. Comp. 725 (2017) 1238–1243.